

## Enhancement of Interdecadal Climate Variability in the Sahel by Vegetation Interaction

Ning Zeng,<sup>1\*</sup> J. David Neelin,<sup>1</sup> K.-M. Lau,<sup>2</sup> Compton J. Tucker<sup>2</sup>

The role of naturally varying vegetation in influencing the climate variability in the West African Sahel is explored in a coupled atmosphere–land–vegetation model. The Sahel rainfall variability is influenced by sea-surface temperature variations in the oceans. Land-surface feedback is found to increase this variability both on interannual and interdecadal time scales. Interactive vegetation enhances the interdecadal variation substantially but can reduce year-to-year variability because of a phase lag introduced by the relatively slow vegetation adjustment time. Variations in vegetation accompany the changes in rainfall, in particular the multidecadal drying trend from the 1950s to the 1980s.

The rainfall over the West African Sahel region (1) shows a multidecadal drying trend from the 1950s to the 1980s and early 1990s, as well as strong interannual variability (Fig. 1A). Causes proposed to explain this dramatic trend include global sea surface temperature (SST) variations (2–5) and land use change, that is, the desertification process (6, 7). Because vegetation dis-

tribution tends to be controlled largely by climate (8, 9), and surface property changes can affect climate by modifying the atmospheric energy and water budget (10–13), it is reasonable to propose that dynamic vegetation–climate interaction might influence decadal climate variability substantially in a climatically sensitive zone such as the Sahel. We tested this

## REPORTS

hypothesis in a coupled atmosphere–land–vegetation model of intermediate complexity.

The atmospheric component of the model is the Quasi-equilibrium Tropical Circulation Model (QTCM) (14, 15), which is coupled to the land surface model Simple-Land (SLand) (15). The QTCM simulates a seasonal climate over the Sahel that is close to observations and that compares favorably with current atmospheric general circulation models (GCMs). We modeled the major effects of a varying vegetation on climate through its control of the evapotranspiration process and modification of surface albedo with SLand. Other effects, such as surface roughness and modification of soil properties, were not considered.

Vegetation growth in the tropics responds mostly to the interannual variations of water availability and is less influenced by temperature and nutrient limitation on these time scales because of the relatively large rainfall variability there. The central equation in the dynamic vegetation model is a biomass equation driven by photosynthesis and vegetation loss

$$\frac{dV}{dt} = a\beta(w)(1 - e^{-kL}) - V/\tau \quad (1)$$

where  $t$  is time,  $a$  is a carbon assimilation coefficient,  $\beta$  is the soil moisture dependence as used in the original SLand,  $w$  is soil wetness,  $L$  is the plant leaf area index (LAI), and  $k$  is the extinction coefficient of photosynthetically active sunlight taken as 0.75. The vegetation time scale  $\tau$  is set to 1 year. This equation is similar to the biomass equations used in models with more explicit vegetation dynamics (16–19).  $V$  is interpreted as vegetation amount or leaf biomass, and it is normalized between 0 and 1. The LAI is assumed to be directly proportional to  $V$  as  $L = L_{\max}V$ , where  $L_{\max}$  is a maximum LAI of 8. The carbon assimilation coefficient  $a$  takes a value such that  $V = 1$  at equilibrium ( $dV/dt = 0$ ) and without water stress ( $\beta = 1$ ). This model does not explicitly include plant competition nor does it consider species-specific characteristics such as resource allocation. Seasonality is not explicitly modeled for  $V$ , so Eq. 1 represents variation on the background of a mean seasonal cycle.

The original version of the land model was modified to account for the effects of leaf-to-canopy scaling (20) so that the canopy conductance  $g_c$  for evapotranspiration is

$$g_c = g_{\max}\beta(w)(1 - e^{-kL})/k \quad (2)$$

where  $g_{\max}$  is a leaf-level maximum conductance. Note that photosynthesis and evapotranspiration are closely related in Eqs. 1 and 2 (20). Besides modifying evapotranspiration through Eq. 2, vegetation also changes land surface albedo  $A$  as (21)

$$A = 0.38 - 0.3(1 - e^{-kL}) \quad (3)$$

This corresponds to an albedo of 0.38 at  $V = 0$  (desert) and 0.08 at maximum vegetation  $V = 1$  (dense forest). Thus, vegetation feeds back into the atmosphere by modifying evapotranspiration and surface albedo through Eqs. 2 and 3.

In order to identify the relative importance of oceanic forcing as represented by SST, land surface, and vegetation processes, we performed a series of model experiments, starting from a run in which both land and vegetation were interactive. In this realistic case, designated AOLV, the atmosphere, ocean, land, and vegetation all contribute to variability. The monthly output from this run was then used to derive a vegetation climatology that has a seasonal cycle but does not change from year to year, which was used as a model boundary condition for the second run, designated AOL. The output of the run AOL was then used to derive a soil moisture climatology that was used to drive the third experiment, AO. In all these three runs, the coupled atmosphere–land–vegetation model is driven by the observed monthly SST from 1950 to 1998 (22). All three start from an initial condition taken from an interactive land-vegetation run forced by a climatological SST. The modeled annual rainfall over the Sahel from these experiments is shown in Fig. 1, B through D.

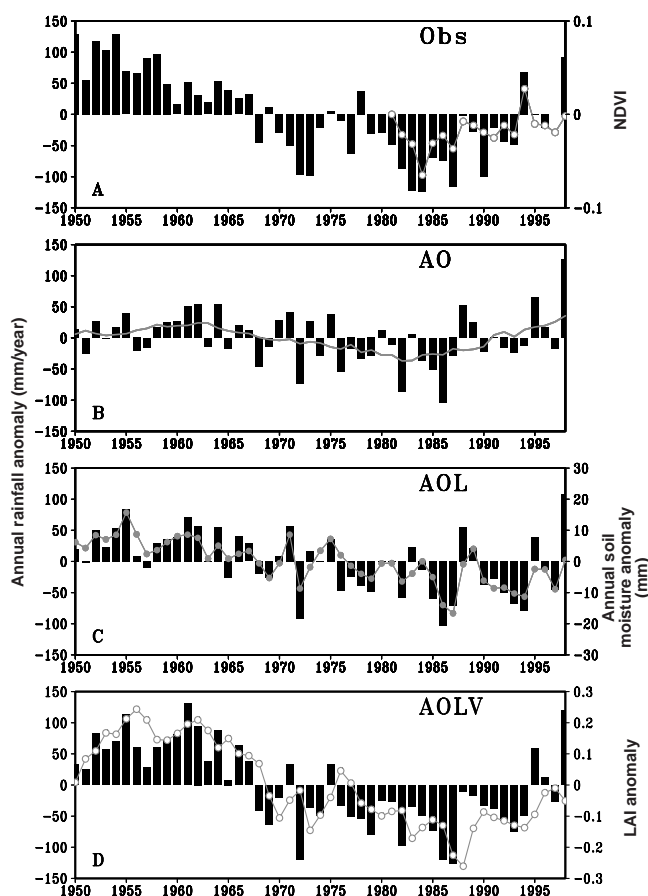
Compared to the observations in Fig. 1A, the AO run forced by interannually varying SST but with noninteractive soil moisture and vegetation (Fig. 1B) shows a weak interannual variation and a much weaker interdecadal signal, although a drying trend can be seen from the 1950s to the 1980s. The interactive soil moisture (Fig. 1C) appears to increase this interdecadal drying trend into the early 1990s. The simulated soil moisture shows a high degree of correlation with precipitation. The amplitude of interannual variation is also larger in general, in agreement with other studies (23–25).

Allowing vegetation feedback to the atmosphere in AOLV substantially enhances the decadal rainfall variability (Fig. 1D). The wet periods in the 1950s and the dry periods in the 1970s and the 1980s stand out and are more like observations of actual conditions. Compared to the noninteractive vegetation case, AOL, the interannual variability does not show enhancement. In some cases, the year-to-year change, such as from the dry 1987 to the relatively wet 1988, is actually reduced because the slowly responding vegetation is still low from the previous drought. This complicated lagged rela-

<sup>1</sup>Department of Atmospheric Sciences and Institute of Geophysics and Planetary Physics, University of California, Los Angeles, CA 90095–1565, USA. <sup>2</sup>NASA-Goddard Space Flight Center, Greenbelt, MD, 20771, USA.

\*To whom correspondence should be addressed. E-mail: zeng@atmos.ucla.edu

**Fig. 1.** Annual rainfall anomaly (vertical bars) over the West African Sahel (13N–20N, 15W–20E) from 1950 to 1998. (A) Observations from Hulme (7). (B) Model with noninteractive land surface hydrology (fixed soil moisture) and noninteractive vegetation (SST influence only, AO). Smoothed line is a 9-year running mean showing the low-frequency variation. (C) Model with interactive soil moisture but noninteractive vegetation (AOL). (D) Model with interactive soil moisture and vegetation (AOLV). Also plotted (as connected circles, labeled on the right) are (A) the normalized difference vegetation index (NDVI) (37), (C) the model simulated annual soil moisture anomaly, and (D) the model simulated LAI anomaly. All the anomalies are computed relative to the 1950–98 base period, except that the NDVI data is relative to 1981.



## REPORTS

tionship between vegetation and precipitation is also seen in the observations (26), but our understanding of vegetation dynamics and the modeling tools available are not sufficient for a precise assessment of the reasons for this. Variation in rainfall drives a similar trend in vegetation through vegetation growth or loss (Fig. 1D). The vegetation lags slightly behind the rainfall, and its variation is also smoother, although these tendencies are not very strong, because the 1-year vegetation time scale used in the model runs is comparable to the time resolution of the plot.

To assess the internal climate variability in the model, additional nine-member ensemble runs have been conducted corresponding to each of the three cases above. The member runs in an ensemble differ only in their initial atmospheric and soil moisture conditions. We used the Sahel rainfall difference between the wet period 1950–67 and the dry period 1968–87 as an indicator of the amplitude of the interdecadal variation. Successive amplification of the decadal trend occurs with the inclusion of interactive soil moisture, especially vegetation (Fig. 2). However, even the AOLV ensemble still tends to underestimate the observed decadal trend, and the case shown in Fig. 1D is on the high side of the distribution. Furthermore, the scatter among the ensemble members also increases when additional feedbacks are included. Interactive vegetation increases the variance even though initial vegetation conditions are identical in these runs.

The interactive vegetation modifies the precipitation through a chain of positive feedback loops. For instance, decreased rainfall leads to less water availability and reduces vegetation, which in turn leads to higher surface albedo and reduced evapotranspiration. This weakens the large-scale atmospheric circulation by reducing the energy and water flux into the atmosphere column, thus further decreasing the local rainfall (6, 10, 12, 27).

The dynamic nature of the vegetation-climate interaction can be understood more precisely in a linear system by simplifying these feedback processes

$$\frac{dV'}{dt} = \frac{\alpha P' - V'}{\tau} \quad (4)$$

$$P' = \mu V' + F_0 e^{i\omega t} \quad (5)$$

Here  $V'$  and  $P'$  are perturbations in vegetation and precipitation, respectively, and they approximate the interannual and interdecadal anomalies shown above. The coefficients  $\alpha$  and  $\mu$  represent the strength of the local interaction between vegetation and the atmosphere. Equation 4 is a linearized version of the biomass equation (Eq. 1) because soil moisture is forced by precipitation. A similar expression was derived by Brovkin *et al.* (28). Equation 5 approximates the vegetation feedback to rainfall through changes in surface albedo in Eq. 3 and evapotranspiration in Eq. 2. Rainfall is sinusoidally forced at a frequency  $\omega$  and an amplitude  $F_0$ , representing the SST-induced change in the large-scale atmospheric circulation.

The dependences on  $\omega$  of the amplitude of  $P'$  and phase lag  $\phi$  are shown in Fig. 3 (29). At low-frequency forcing ( $\omega\tau \rightarrow 0$ ), vegetation has enough time to establish a near equilibrium with the precipitation, so the precipitation is enhanced by a factor of  $1/(1 - \alpha\mu)$  with little phase lag. This explains the amplification of the interdecadal variation of rainfall shown in Fig. 1D. At high-frequency forcing ( $\omega\tau \rightarrow \infty$ ), vegetation has little time to respond to the forcing because of its relatively long adjustment time; therefore, the precipitation variation is mostly a direct response to the forcing. At intermediate-frequency forcing, the amplitude is enhanced slightly, but the phase lag is at a maximum. This phase lag has significant consequences for the interannual variability. In 1988, for instance, the memory in vegetation of the previous drought years has delayed and reduced the otherwise strong wetting tendency resulting from SST-induced atmospheric circulation change (Fig. 1, C and D).

The modeled Sahel rainfall in AOLV shows a correlation with observations of 0.67, a significant improvement from a 0.44 correlation in AOL. However, the year-to-year comparison with the observations is not as satisfactory. When we decompose the Sahel rainfall time series into low-frequency

(longer than 10 years) and high-frequency (shorter than 10 years) components, the correlation with the observation is only 0.1 at high frequency and 0.94 at low frequency for the AOLV run. The discrepancy in the interannual simulation, both in our model and in the GCMs (4, 30), may have a considerable contribution from chaotic atmospheric internal variability, for which model and observation can only be compared in a statistical sense.

Although we focus on natural climate variations involving vegetation change, this does not exclude any role anthropogenic land use change might play. It is possible that desertification might account for the remaining difference between the interactive vegetation run and observations in Fig. 2 on decadal time scales, but because the vegetation feedback acts to amplify Sahel rainfall variability that originates from SST variations, significant effects can occur with relatively small vegetation changes. The change of surface albedo (not shown in Fig. 1) on the interdecadal time scale is about 0.03 in the experiment with interactive vegetation (AOLV). This is a subtle change compared either to the albedo change values of 0.1 used in GCM desertification experiments (6) or to what could be estimated from satellite observations in earlier decades. Current satellite systems will be capable of measuring this level of variation for future decadal fluctuations. The present results suggest the importance of such measurements because of the role vegetation feedbacks can play in interannual and interdecadal climate variability in climatically sensitive zones such as the Sahel.

**Fig. 2.** Sahel rainfall difference between the period 1950–67 and the period 1968–87 for observations (solid square) and for three nine-member ensemble runs with and without interactive soil moisture and vegetation, similar to the ones in Fig. 1, B through D. Open circles denote individual ensemble members with different initial conditions and hence different chaotic internal variability. Crosshairs denote ensemble means.

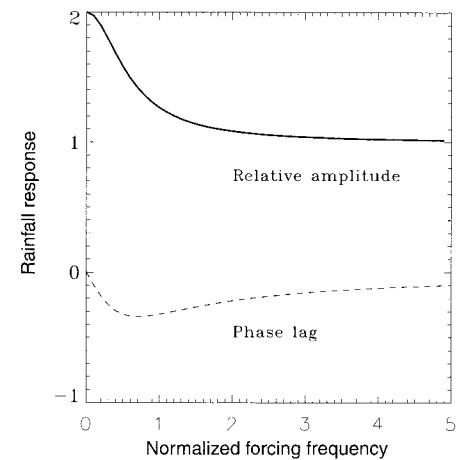
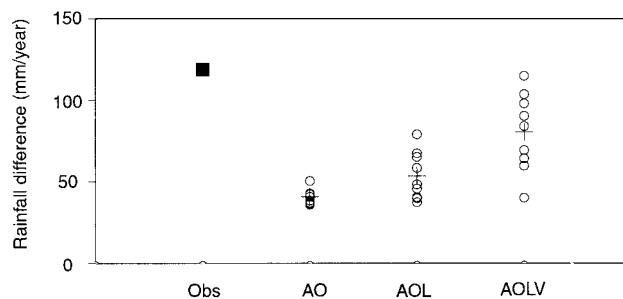


**Fig. 3.** Response of rainfall to a sinusoidal forcing in the idealized linear system (Eqs. 4 and 5), illustrating the dependence of vegetation feedback on forcing frequency. The response amplitude ( $P'/F_0$ , solid line) and phase lag ( $\phi$ , in radians; dashed line) are plotted as a function of the forcing frequency  $\omega\tau$  (normalized by the vegetation time scale  $\tau$ ).

## REPORTS

### References and Notes

1. Rainfall, based on the surface gauge data from M. Hulme [in *Global Precipitations and Climate Change*, M. Desbois and F. Desalmand, Eds. (NATO ASI Series, Springer-Verlag, Berlin, 1994), pp. 387–406], averaged over 15W–20E, 13N–20N, which approximately corresponds to the Sahel region as defined by S. E. Nicholson [in *Natural Climate Variability on Decade-to-Century Time Scales* (National Research Council, National Academy Press, Washington, DC, 1995), pp. 32–43].
2. C. K. Folland, T. N. Palmer, D. E. Parker, *Nature* **320**, 602 (1986).
3. D. P. Rowell, C. K. Folland, K. Maskell, M. N. Ward, *Q. J. R. Meteorol. Soc.* **121 A**, 669 (1995).
4. D. P. Rowell, *Q. J. R. Meteorol. Soc.* **122**, 1007 (1996).
5. F. H. M. Semazzi, B. Burns, N.-H. Lin, J.-K. Schemm, *J. Climate* **9**, 2480 (1996).
6. Y. Xue and J. Shukla, *J. Climate* **5**, 2232 (1993).
7. P. A. Dirmeyer and J. Shukla, *Q. J. R. Meteorol. Soc.* **122**, 451 (1996).
8. L. R. Holdridge, *Science* **105**, 367 (1947).
9. F. I. Woodward, *Climate and Plant Distribution* (Cambridge Univ. Press, Cambridge, 1987).
10. J. G. Charney, *Q. J. R. Meteorol. Soc.* **101**, 193 (1975).
11. J. Shukla and Y. Mintz, *Science* **215**, 1498 (1982).
12. R. E. Dickinson, in *Climate System Modeling*, K. E. Trenberth, Ed. (Cambridge Univ. Press, Cambridge, 1992), pp. 689–701.
13. M. Claussen, *Global Change Biol.* **4**, 549 (1998).
14. J. D. Neelin and N. Zeng, *J. Atmos. Sci.*, in press.
15. N. Zeng, J. D. Neelin, C. Chou, *J. Atmos. Sci.*, in press.
16. H. H. Shugart, *A Theory of Forest Dynamics: The Ecological Implications of Forest Succession Models* (Springer-Verlag, New York, 1984).
17. J.-J. Ji, *J. Biogeogr.* **22**, 445 (1995).
18. J. A. Foley et al., *Global Biogeochem. Cycles* **10**, 603 (1996).
19. R. E. Dickinson, M. Shaikh, R. Bryant, L. Graumlich, *J. Climate* **11**, 2823 (1998).
20. P. J. Sellers et al., *J. Climate* **9**, 676 (1996).
21. M. Verstraete, B. Pinty, R. E. Dickinson, *J. Geophys. Res.* **95**, 755 (1990).
22. R. W. Reynolds and T. M. Smith, *J. Climate* **7**, 929 (1994).
23. T. L. Delworth and S. Manabe, *Adv. Water Resour.* **16**, 3 (1993).
24. R. D. Koster and J. J. Suarez, *J. Geophys. Res.* **100**, 13775 (1995).
25. K.-M. Lau and W. Bua, *Clim. Dyn.* **14**, 759 (1998).
26. S. N. Goward and S. D. Prince, *J. Biogeogr.* **22**, 549 (1995).
27. N. Zeng and J. D. Neelin, *J. Climate* **12**, 857 (1999).
28. V. Brovkin, M. Claussen, V. Petoukhov, A. Ganopolski, *J. Geophys. Res.* **103**, 31613 (1998).
29. The solutions of Eqs. 4 and 5 for the oscillation amplitude and phase shift  $\phi$  relative to the forcing for  $P'$  are
 
$$\left| \frac{P'}{F_0} \right|^2 = \frac{1 + \omega^2 \tau^2}{(1 - \alpha\mu)^2 + \omega^2 \tau^2}$$

$$\tan(\phi) = -\frac{\alpha\mu\omega\tau}{1 - \alpha\mu + \omega^2 \tau^2}$$

For conditions on the approximations in Eq. 5, see (27). The coupling coefficients  $\alpha$  and  $\mu$  are positive and  $\alpha\mu < 1$  so that the positive feedbacks do not become unstable. In Fig. 3,  $\alpha\mu = 0.5$ .

30. K. R. Sperber and T. N. Palmer, *J. Climate* **9**, 2727 (1996).
31. C. J. Tucker and S. E. Nicholson, *Ambio* **28**, 587 (1999).
32. Supported by NSF grant ATM-9521389, NOAA grant NA86GP0314, and a grant to N.Z. from the NASA IPA program. We thank two anonymous reviewers for their constructive comments, K. Hales for help with the rainfall data, M. Cisse for processing the normalized difference vegetation index data, and V. Nelson for editorial assistance.

14 July 1999; accepted 6 October 1999